

# Flux trapping in NbTiN strips and structures

Ruiheng Bai

*Laboratory of Atomic and Solid State Physics, Cornell University, Ithaca, NY, USA*

Aliakbar Sepehri and Yen-Lee Loh

*Department of physics, University of North Dakota, Grand Forks, ND, USA*

Anne-Marie Valente-Feliciano

*Thomas Jefferson National Accelerator Facility, Newport News, VA, USA*

Anna Herr and Quentin Herr

*imec USA, Kissimmee, FL, USA*

Katja C. Nowack\*

*Laboratory of Atomic and Solid State Physics, Cornell University, Ithaca, NY, USA and  
Kavli Institute at Cornell for Nanoscale Science, Ithaca, New York 14853, USA*

(Dated: March 19, 2025)

We use scanning superconducting quantum interference device (SQUID) microscopy to image vortices in superconducting strips fabricated from NbTiN thin films. We repeatedly cool superconducting strips with different width in an applied magnetic field and image the individual vortices. From these images we determine the threshold field at which the first vortex enters a strip, as well as the number and spatial configuration of vortices beyond this threshold field. We model vortex behavior with and without considering the effect of pinning by numerically minimizing the Gibbs free energy of vortices in the strips. Our measurements provide a first benchmark to understand the flux trapping properties of NbTiN thin films directly relevant to NbTiN-based superconducting circuits and devices.

## I. INTRODUCTION

Understanding and characterizing the behavior of vortices in fabricated superconducting structures is important for a range of applications including superconducting digital circuits (SDCs), on-chip resonators in superconducting quantum information devices, and detectors for radiation across a wide range of wavelengths. In thin-film superconductors pinned or trapped vortices are typically present even at very low fields. However, in finite-sized structures, the energy landscape for vortices is altered due to the presence of edges, leading to behavior that deviates from that observed in continuous films. For example, the threshold field required for the first vortex to enter and the spatial distribution of subsequent vortices depend not only on pinning sites and the intrinsic properties of the superconductor but also on the geometry of the structure. A superconducting strip serves as a simple technologically-relevant example for studying these effects.

Experimentally, the behavior of vortices in strips has been explored by Stan et al. [1] in Nb, Kuit et al. [2] in YBCO, Ceccarelli et al. [3] in amorphous MoSi, and Ge et al. [4] in Pb strips. In these studies, images of the vortex configurations as a function of the applied field were acquired using various local magnetometry techniques. From these images, the number of vortices in a

given strip as a function of field can be extracted. Refs. [1, 2, 4] predominantly focused on the threshold field and its dependence on strip width as in more detail described below.

Theoretically, several models to predict the threshold field have been proposed, but only limited work has focused on the behavior of vortices beyond the threshold field and the effect of pinning on the threshold field. Bronson et al. [5] addressed this problem and implemented a simple numerical model to predict vortex configuration in a superconducting strip including vortex-vortex interactions and the effect of pinning. A summary of the theoretical work is presented below.

In this work, we combine detailed measurements with modeling of vortex behavior in NbTiN strips. We use scanning SQUID microscopy to image the vortex configurations in the strips as a function of an applied magnetic field. We perform simulations to capture the threshold field and the dependence of the number of vortices as a function of field beyond the threshold field. These simulations are directly based on models described by Bronson et al. [5] with modifications to include the finite length of our superconducting strips and to consider a modified self-energy of the vortices (see supplementary materials for details [6]).

We focus on NbTiN due to its promise for scaling wires, vias, Josephson junctions, capacitors, and ground planes in a superconducting digital circuit (SDC) fabrication stack [7–10]. To date most efforts in SDCs have centered on Nb-based circuits. Nb is an elemental su-

\* kcn34@cornell.edu

perconductor with a critical temperature of 9.2 K, thin films can be readily produced using DC sputtering and structures can be patterned by conventional etch processes. However, it is challenging to achieve sub 250 nm feature sizes and reproducible circuit performance using Nb. Major limitations include unstable material properties caused by complex oxidation, and a related low processing temperature requirement which leads to the degradation of the superconducting properties of SDCs due to the cumulative effects of fabrication processing [10].

Compared to Nb, NbTiN has a higher critical temperature of up to 17.3 K and high stability allowing for high processing temperatures up to 1,000 °C both depending on the composition which is controlled during the deposition. NbTiN wires with stable superconducting properties down to a  $10 \times 10 \text{ nm}^2$  cross-section, a critical temperature up to 15 K and a critical current density of  $100 \text{ mA}/\mu\text{m}^2$  have been demonstrated [7]. In addition, NbTiN has a low microwave surface resistance leading to reduced microwave losses compared to Nb.

A challenge for SDCs is circuit failure due to uncontrolled flux trapping, which leads to variations of circuit behavior from cooldown to cooldown. For NbTiN thin films, no direct measurements of the flux trapping properties are available. Our measurements presented here provide a first benchmark to investigate the flux trapping properties of NbTiN thin films directly relevant to NbTiN-based SDCs.

This paper is organized as follows. In Sec. II and III, we describe the experimental and theoretical methods used in this study. Then in Sec. IV, we extract the threshold field values from magnetic images of the strips cooled in different magnetic field and compare the threshold field values with various models. In Sec. V, we compare experimental results of vortex trapping in strips above threshold field with models considering and not considering pinning. We conclude in Sec. VI.

## II. SAMPLES AND EXPERIMENTAL METHODS

A nominally 50 nm thick NbTiN film was deposited using a PVD tool and patterned with 193 nm immersion lithography. We study two samples, S1 and S2, originating from the same 300 mm wafer with S1 coming from the middle between center and edge of the wafer, and S2 from the center. The properties of the film vary as a function of distance from the center [9]. On a wafer grown under the same conditions the room temperature resistivities are  $246 \mu\Omega\text{cm}$  and  $291 \mu\Omega\text{cm}$  at positions approximately corresponding to S1 and S2, and  $T_c$  of 13.5 K and 12.6 K, respectively. Both samples have a set of strips with width varying from  $2.5 \mu\text{m}$  to  $40 \mu\text{m}$ , and a length of  $200 \mu\text{m}$ . Based on the resistivity, the London penetration depth is estimated to be approximately  $500 - 570 \text{ nm}$  for the type of films studied [11].

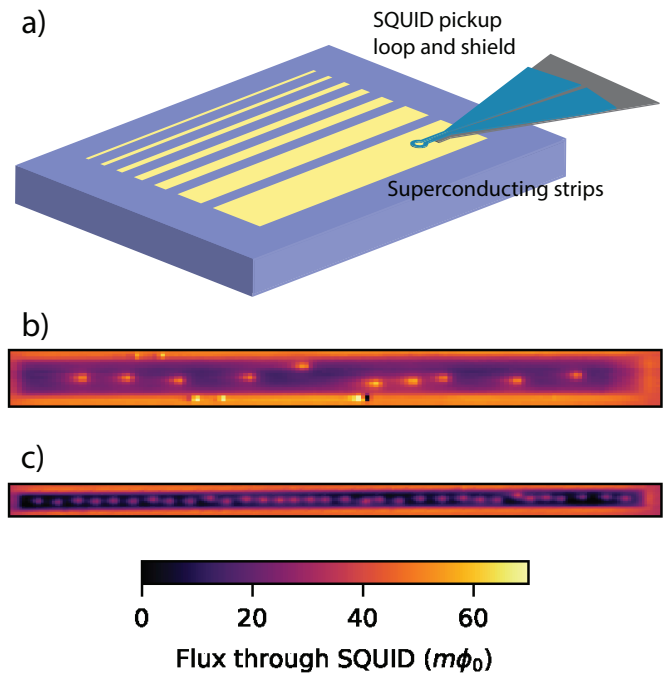


**FIG. 1:** (a) Schematic of the SQUID pickup loop positioned above the NbTiN strip to image the stray magnetic field produced by trapped vortices. (b,c) Images of superconducting strips with width (b)  $20 \mu\text{m}$  (cooled in  $16 \mu\text{T}$  field) and (c)  $10 \mu\text{m}$  (cooled in  $80 \mu\text{T}$  field). Colorbar is identical for both images.

We use scanning SQUID microscopy to image vortices in our samples. The SQUID sensor has a pickup loop with an inner and outer diameter of approx.  $0.75 \mu\text{m}$  and  $1.6 \mu\text{m}$ , respectively. The pickup loop is scanned approximately at  $1 \mu\text{m}$  height above the sample. A low-field magnet coil surrounding the cryostat provides control over the out-of-plane magnetic field. The sample is mounted on a stage with only weak thermal coupling to the cryostat, and a heater and thermometer near the sample on this stage allow us to adjust its temperature independent of the cryostat and SQUID temperature.

Unless noted otherwise, our measurements are performed in the following way. First, we heat the sample above its critical temperature and adjust the out-of-plane magnetic field. Then, we cool the sample to approx. 8 K while maintaining the field. At 8 K, the vortices become immobile, and we acquire magnetic images to determine the number and positions of the trapped vortices.

Figs. 1 b) and c) show representative images of superconducting strips with widths of  $20 \mu\text{m}$  and  $10 \mu\text{m}$  after field cooling in  $16 \mu\text{T}$  and  $80 \mu\text{T}$ , respectively. In these images, individual vortices are clearly visible as bright dots, while the overall strip appear darker than the surrounding area due to the Meissner effect screening the applied magnetic field. The slight tear-drop shape of the vortices is due to the details of the geometry of the SQUID's pickup loop [12, 13]: the pickup loop connects

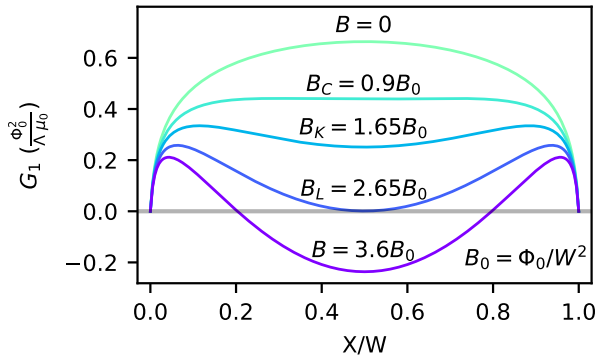


**FIG. 2:** Gibbs free energy in units of  $\Phi_0^2/(\Lambda\mu_0)$  for a single vortex at position  $X$  in a strip of width  $W$  for  $r_c/W = 0.01$ . The curves, shown for various applied field values, include those corresponding to the different models of the threshold field defined in the main text.

via two leads to the main SQUID body, and magnetic flux couples into a small unshielded opening between these leads causing a deviation from a circular shape of the sensitive area. Acquiring such images as a function of applied magnetic field allows us to extract the threshold field, the number of vortices as a function of field, and the spatial distribution of vortices for strips with different width.

### III. DESCRIBING VORTICES IN AN INFINITE SUPERCONDUCTING STRIP

To model the behavior of vortices in our NbTiN strips, we begin by assuming that our films are in the 2D limit, i.e. the penetration depth  $\lambda$  is much larger than the film thickness  $d$ . In this regime, vortices take the form of Pearl vortices [14], and the Pearl length is given by  $\Lambda = 2\lambda^2/d$ . A Pearl vortex in an infinite film consists of three regions: a core ( $r \lesssim r_c$ ) in which the circulating sheet current  $K$  increases as  $K \sim r$ ; an intermediate region ( $r_c \lesssim r \lesssim \Lambda$ ) where  $K \sim 1/r$ ; and an outer region ( $r \gg \Lambda$ ) where  $K \sim 1/r^2$ . In our NbTiN films, we expect that near  $T_c$  when vortices are trapped that the vortex core radius is much smaller than the Pearl length,  $r_c \ll \Lambda$ . Under this assumption, vortices can be modelled as pointlike particles whose behavior is determined by their Gibbs free energy.

The Gibbs free energy for a finite number of vortices in a superconducting strip of width  $W$  consists of the single vortex energies and their interactions. Kogan analytically obtained the energy and magnetic moment of a vortex near the edge of a semi-infinite thin superconducting film and in an infinite thin-film strip [15] assuming  $\Lambda \gg W$ . We first consider an infinite strip with its long direction along the  $y$  axis and its width along the  $x$  axis

with bounds  $0 < X < W$ . With that the Gibbs free energy of a single vortex at position  $(X, Y)$  is given by [5, 15]:

$$G_1(X, Y) = F(X, Y) - m(X, Y)B. \quad (1)$$

where  $B$  is the applied magnetic field normal to the superconducting strip,  $m(X, Y)$  is the magnetic moment of the vortex, and  $F(X, Y)$  is the free energy of the vortex including self-energy and edge screening effects. Fig. 2 shows this Gibbs free energy  $G_1$  of a single vortex as a function of applied magnetic field, where we use the following expression for  $m(X, Y)$  and  $F(X, Y)$ :

$$m(X, Y) = \frac{\Phi_0}{\mu_0\Lambda}X(W - X), \quad (2)$$

where  $\Phi_0 = h/2e$  is the flux quantum [16], and  $\mu_0$  the vacuum permeability. and

$$F(X, Y) = \frac{\Phi_0^2}{2\pi\mu_0\Lambda} \ln \left[ \frac{2W}{\pi r_c} \sin\left(\frac{\pi X}{W}\right) + 1 \right]. \quad (3)$$

Our expression for  $F(X, Y)$  includes two modifications compared to previous work. First, we include  $r_c$  as the effective vortex core radius to avoid identification with the coherence length  $\xi$ . While  $\xi$  and  $r_c$  are related, they are not identical in particular in a thin film superconductor in the Pearl limit. We treat  $r_c$  as a material parameter that characterizes the free energy of a vortex. Second, the additional  $' + 1'$  ensures that  $F(X, Y)$  is zero at the edges of the strip at  $X = 0$  and  $X = W$ .

To understand the behavior of vortices beyond the threshold field at which the first vortex enters, we need to include the energy associated with interactions between vortices. For two vortices of the same polarity at positions  $(X, Y)$  and  $(x, y)$  this energy is given by:

$$G_2(X, Y; x, y) = \frac{\Phi_0^2}{2\pi\mu_0\Lambda} \ln \left[ \frac{\cos \frac{\pi(x+X)}{W} - \cosh \frac{\pi(y-Y)}{W}}{\cos \frac{\pi(x-X)}{W} - \cosh \frac{\pi(y-Y)}{W}} \right]. \quad (4)$$

To study the effect of pinning, energy terms can be included that model localized pinning sites. A common way to model pinning is to include terms that lower the free energy of a vortex at random locations in the strip. These terms compete with vortex-vortex interactions that tend to produce an ordered arrangement of vortices, and they will lower the threshold field required to induce the first vortex in a strip. We present a toy model that requires numerical simulations based on a model by Bronson et al. in section V to account for the effect of pinning in our experiments.

### IV. THRESHOLD FIELD FOR INDUCING THE FIRST VORTEX IN SUPERCONDUCTING NBTIN STRIPS

From Fig. 2 it is clear that in the absence of pinning, the first vortex is expected to settle in the center of the

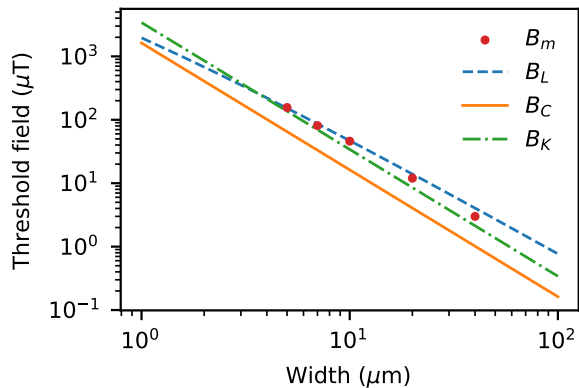


**FIG. 3:** Threshold field  $B_m$  extracted from images alongside the model predictions  $B_C$ ,  $B_K$  and  $B_L$ . Fitting  $B_L$  to the data yields a best-fit value of  $r_c = 185 \pm 11$  nm.

strip, where the Gibbs free energy develops a local minimum as the magnetic field increases. Several models have been proposed for the threshold field in the absence of pinning. Likharev proposed that the first vortex in a strip is trapped once it is absolutely stable [17]. This corresponds to the field at which the Gibbs free energy in eq. 1 becomes zero or smaller, first happening at the center of the strip. This condition leads to

$$B_L = \frac{2\Phi_0}{\pi W^2} \ln \frac{2W}{\pi r_c} + 1. \quad (5)$$

$B_L$  reflects the competition between the magnetic energy and the self-energy of a vortex in the strip, and it is independent of  $\Lambda$  because both contributions scale identically with  $\Lambda$ .

Clem [18] proposed an alternative criterion, defining the threshold field as the field at a local minimum first appears in the Gibbs free energy, rendering the vortex metastable. This criterion leads to

$$B_C = \frac{\pi\Phi_0}{4W^2} \quad (6)$$

Kuit et al. [2] introduced a model that incorporates the generation of vortex-antivortex pairs just below the critical temperature, in addition to the contributions considered in the previous section. Their analysis yields

$$B_K = 1.65 \frac{\Phi_0}{W^2} \quad (7)$$

Notably,  $B_K$  and  $B_C$  solely depend on the width of the strip  $W$ , whereas  $B_L$  includes an additional logarithmic dependence on the ratio  $W/r_c$ . Experimentally, we identify the threshold field  $B_m$  as the highest field in which a strip is cooled without inducing a vortex. In Fig. 3, we compare the threshold fields of strips with different width  $W$  from S2 to the predictions of these models. We focus on S2 because, as we discuss below, S1 traps a

small number of vortices at fields significantly below the expected threshold fields, likely due to the presence of a few strong pinning sites. Our method for determining  $B_m$  differs from previous studies [1, 2, 4], which extrapolate the high field linear dependence to zero vortices in the strip. Such an extrapolation underestimates the observed threshold field [5] as we will further show below.

In Fig. 3,  $B_m$  decreases with increasing width reflecting that the effect of the edges becomes less significant. When comparing  $B_m$  to the three models,  $B_C$  underestimates the threshold field for all widths, whereas  $B_K$  and  $B_L$  provide reasonable agreement. For  $B_L$ , a fit to eq.5 yields  $r_c = 185 \pm 11$  nm. It is important to note that none of the above expressions account for the effect of pinning, which we discuss in section V.

## V. NUMBER OF VORTICES ABOVE THE THRESHOLD FIELD

In this section, we focus on the behavior of vortices as a function of applied field beyond  $B_m$  as additional vortices are trapped in the strips during cooling. Fig. 4 shows the number of vortices extracted from images as a function of field for strips with width ranging from 5 to 40  $\mu\text{m}$  in S1 and S2. At high fields, the number of vortices increases linearly with the applied field, but the slope is lower than the slope expected for adding one vortex per  $\Phi_0$  threading the total area  $A$  of the strip, i.e.  $N = (A/\Phi_0)B$ .

Approaching  $B_m$  from above, we observe a shoulder in the curves for the 5, 7, and 10  $\mu\text{m}$  strips and a subtler feature for the 20  $\mu\text{m}$  strip. As the field is lowered further, the strips for S2 show a sharp drop to zero vortices, whereas S1 exhibits a kink for the 5 to 7  $\mu\text{m}$  strips, followed by a shallow tail before reaching zero. Aside from the shallow tail in S1, the number of vortices for both samples are nearly identical.

As we discuss in the modeling section below, without pinning, one expects a steep initial increase in the number of vortices in the center of the strip until vortices come within  $W$  of each other, at which point the slope softens giving rise to the shoulder. As such the shoulder is in line with basic expectations for the vortex behavior, although it has not been clearly resolved in previous studies. Pinning further modifies this simple picture.

Previous studies [1, 2, 4] report similarly a linear dependence at high field. Kuit et al. [2] provide data only for two strip widths with relatively sparse field sampling, making a comparison difficult. The data in Ge et al. [4] shows signatures of the shoulder that we observe, though it is not clearly resolved, and not discussed. Stan et al. [1] observe a transition from a linear dependence to a shallower slope producing a kink similar to our S1 data; however, they do not resolve a shoulder - attributed by Bronson et al. [5] to pinning effects masking the shoulder.  $B_m$  in these studies is determined from extrapolating the high-field linear dependence to zero vortices in the strip,

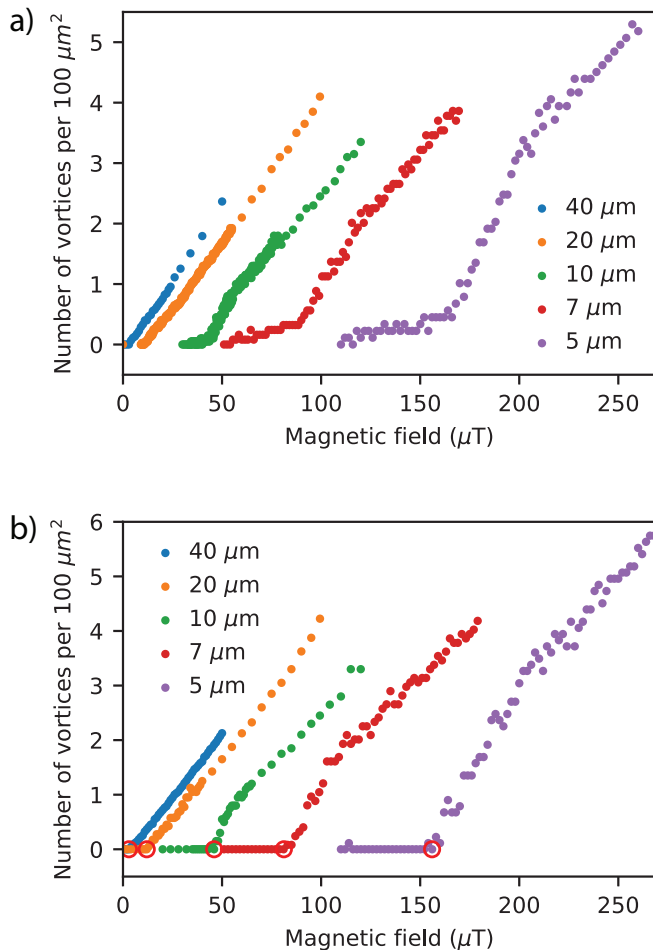


**FIG. 4:** Number of vortices per  $100 \mu\text{m}^2$  trapped in superconducting strip versus value of the applied magnetic field for a) S1, and b) S2. In S1, the presence of more strong pinning sites results in shallow tails at lower magnetic fields. The threshold field values for the S2 strips as shown in Fig. 3 are highlighted by red circles in b).

which systematically underestimates the threshold field.

We next compare our experimental data with two models that capture the interplay of vortex-vortex interactions, finite size and pinning in superconducting strips closely following the approach of Bronson et al. [5]. Both models start from the Gibbs free energy expressions introduced earlier. In the first model, we neglect pinning and assume that the vortices form an ordered lattice within the strip. As the field increases, the number of rows in this lattice is allowed to increase. To explore the influence of pinning near  $B_m$ , we introduce a second, one-dimensional model. In this model, vortices are confined to discrete sites along the center of the strip, and pinning is incorporated by reducing the free energy at selected sites by an energy difference randomly drawn from a distribution. We then use a Metropolis Monte Carlo (MC) algorithm to find the equilibrium vortex configura-

tion for a given applied field.

For the first model, we numerically minimize the Gibbs free energy for various vortex numbers and periodic arrangements of vortices while including vortex-vortex interaction (see Supplemental Material for details [6]). Fig. 5 shows the result for infinite strips of width  $W$  for different values of the ratio  $r_c/W$ . The horizontal axis is normalized by  $B_0 = B \cdot W^2/\Phi_0$ , which represents the field corresponding to one flux quantum per  $W^2$ . The vertical axis shows the number of vortices,  $\tilde{n}$ , in a section of length  $W$  (equivalently a square area  $W^2$ ) within the strip. With this rescaling, the area law corresponds to a line with a slope of 1. The threshold field in the simulated curves corresponds to  $B_L/B_0$ . At the threshold field, the number of vortices steeply increases as vortices first arrange along the center of the strip with equal spacing  $a$ . The curve then rounds over as vortex-vortex interaction become significant, roughly when  $a \approx W$  (or equivalently  $\tilde{n} \approx 1$ ). This behaviour follows from our assumption that  $\Lambda \gg W$ . As the field increases further, additional vortex rows form with regular spacings producing subtle kinks in the simulated curves each time a new row appears.

Experimental data for different strips from S2 nearly collapse onto a single curve when plotted on these rescaled axes, as shown in Fig. 5 a). For comparison, simulated curves corresponding to  $r_c/W$  ratios ranging from 0.185/5 to 0.185/40 (i.e.  $r_c = 185\text{nm}$  and  $W = 5\text{--}40\mu\text{m}$ ) are also shown; here  $r_c = 185\text{nm}$  is the value obtained from fitting the width dependence of the threshold field to  $B_L$  in Fig. 3. Overall, there is good agreement between the data and the simulations, but also discrepancies both close to the threshold field and at higher fields. Close to the threshold field, pinning in the strips is important and is expected to affect the curve, which we will further investigate below.

Generally, one might expect that one value of  $r_c$  characterizes the thin film. Under this assumption, the data for a strip of width  $W$  would follow the curve corresponding to  $r_c/W$ , meaning that wider strips should agree with a lower  $r_c/W$  ratio. This qualitative trend is indeed observed - for example, the data for the  $20\mu\text{m}$  strip fall below those for the  $10\mu\text{m}$  strip. However, none of the experimental curves follows a curve corresponding to a single value of  $r_c/W$ . Especially for  $B/B_0 \gg 1$  (see Fig. 5 b)), the data shifts to larger effective  $r_c/W$ , implying an increasing effective  $r_c$  given that the width of the strip is fixed by lithography. Despite the shift of  $r_c$  with magnetic field, the number of rows of vortices observed in images approximately match the predicted number.

While a detailed understanding of this discrepancy is beyond the scope of this work, we offer a few speculations on its origin. Discrepancies near the threshold field may arise from pinning in the strips, however at higher fields we expect pinning to be less important. One key assumption in our models is that a single value of  $r_c$  and  $\Lambda$  characterizes the strips. Both parameters are temper-

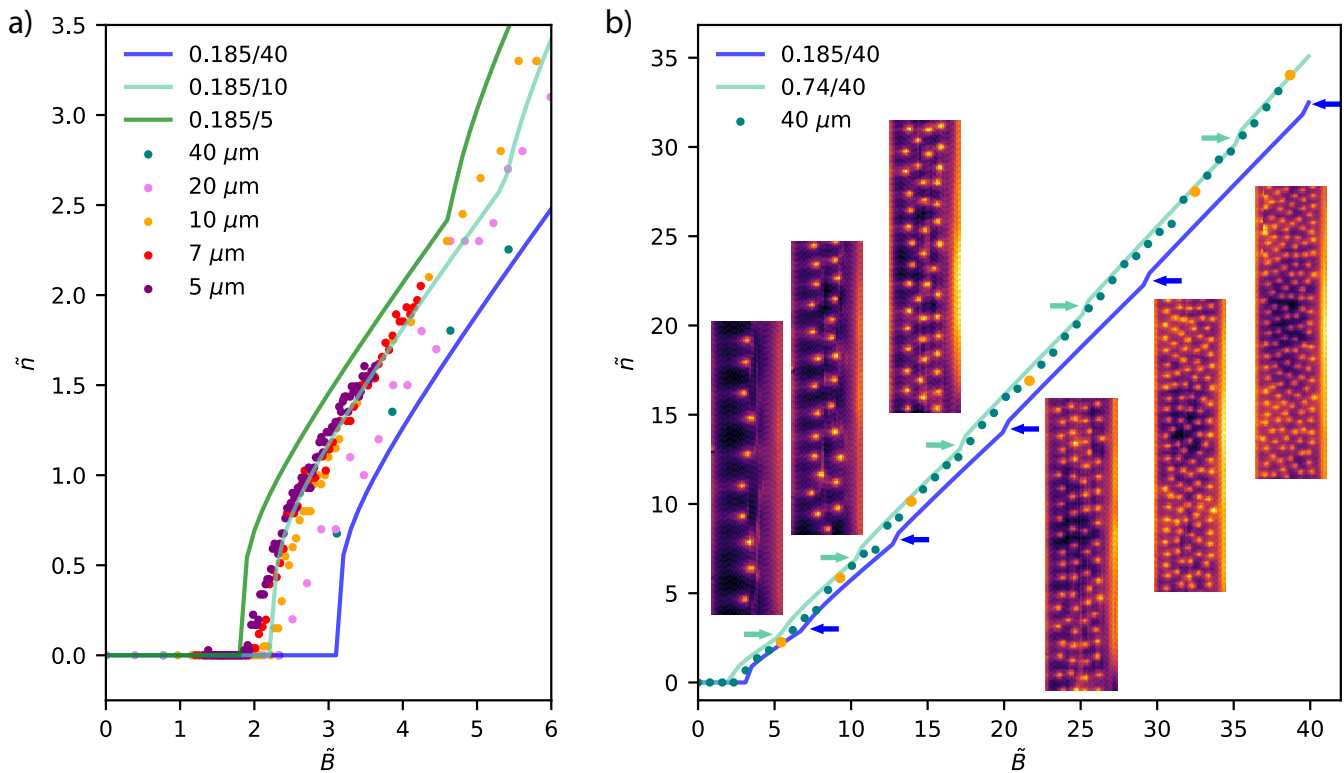


**FIG. 5:** Number of vortices in an area  $W^2$  obtained from model without pinning for different  $r_c/W$  values (solid lines) and experimental data (symbols). Steps in the simulated curves, highlighted by arrows, correspond to an increase of the number of rows by one. Magnetic field is in units of  $B_0$ , i.e.  $\tilde{B} = B/B_0$ . a) shows results for strips of 5 different width on S2 where the  $r_c/W$  values are chosen to correspond to  $r_c = 185\text{nm}$  and  $W = 40\mu\text{m}$ ,  $10\mu\text{m}$  and  $5\mu\text{m}$ . b) shows data for the  $40\mu\text{m}$  strip on S2 over an extended range of  $\tilde{B}$ . Insets show images at the fields highlighted by orange circles.

ature dependent and diverge as  $T_c$  is approached. Our models assume that the relevant values for  $\Lambda$  and  $r_c$  are those at the vortex-freezing temperature, which, according to the literature, is close to  $T_c$ . This implies that  $\Lambda$  and  $r_c$  significantly exceed their low-temperature values, justifying the assumption  $\Lambda \gg W$  used in deriving the Gibbs free energy expressions.

Because vortex capture and freezing is a dynamic process occurring near  $T_c$ , we speculate that the effective  $r_c$  depends on the applied magnetic field. At a fixed field, the Gibbs free energy evolves as the sample cools through the temperature-dependent changes of  $r_c$  and  $\Lambda$ . The observation that, at higher field, the data are consistent with larger  $r_c/W$  ratios suggests that vortices freeze closer to  $T_c$  as the field increases. This trend is consistent with the notion that vortices becoming less mobile in the presence of other vortices. Moreover, from a single vortex perspective, Fig. 2 shows that the energy barrier for a vortex to leave or enter the strip increases with the applied field, further indicating that freezing occurs at temperatures closer to  $T_c$  for higher field. Together, these arguments provide a plausible explanation for why the effective value of  $r_c$  may increase with higher magnetic field.

The second model is aimed at capturing the behavior near the threshold field. In this model, vortices are constrained to discrete sites along the center of the strip, with the number of available sites far exceeding the maximum number of vortices expected at the highest field. Although this model accounts for vortex-vortex interactions, it is only valid in the regime where only a single row of vortices is expected. Without pinning, this model reproduces the same result as the first model at low fields.

To incorporate pinning, additional energy terms are introduced that randomly lower the free energy of a vortex at specific sites along the strip. These terms reduce the threshold field required for the first vortex to enter, broaden the initial steep slope in the number of vortices, and can produce a shallow tail, with all these effects depending on the energies and density of pinning sites. The MC calculations performs exponential cooling - distinct from the experimental cooling procedure - to find the configuration that minimizes the system's energy in the presence of pinning (see supplementary materials [6] for more details).

Figs. 6 a) and d) show simulation results for the  $7\mu\text{m}$  and  $10\mu\text{m}$  strips from S1 and S2, respectively. For both  $7\mu\text{m}$  strips,  $r_c$  is assumed to be  $150\text{nm}$ , while

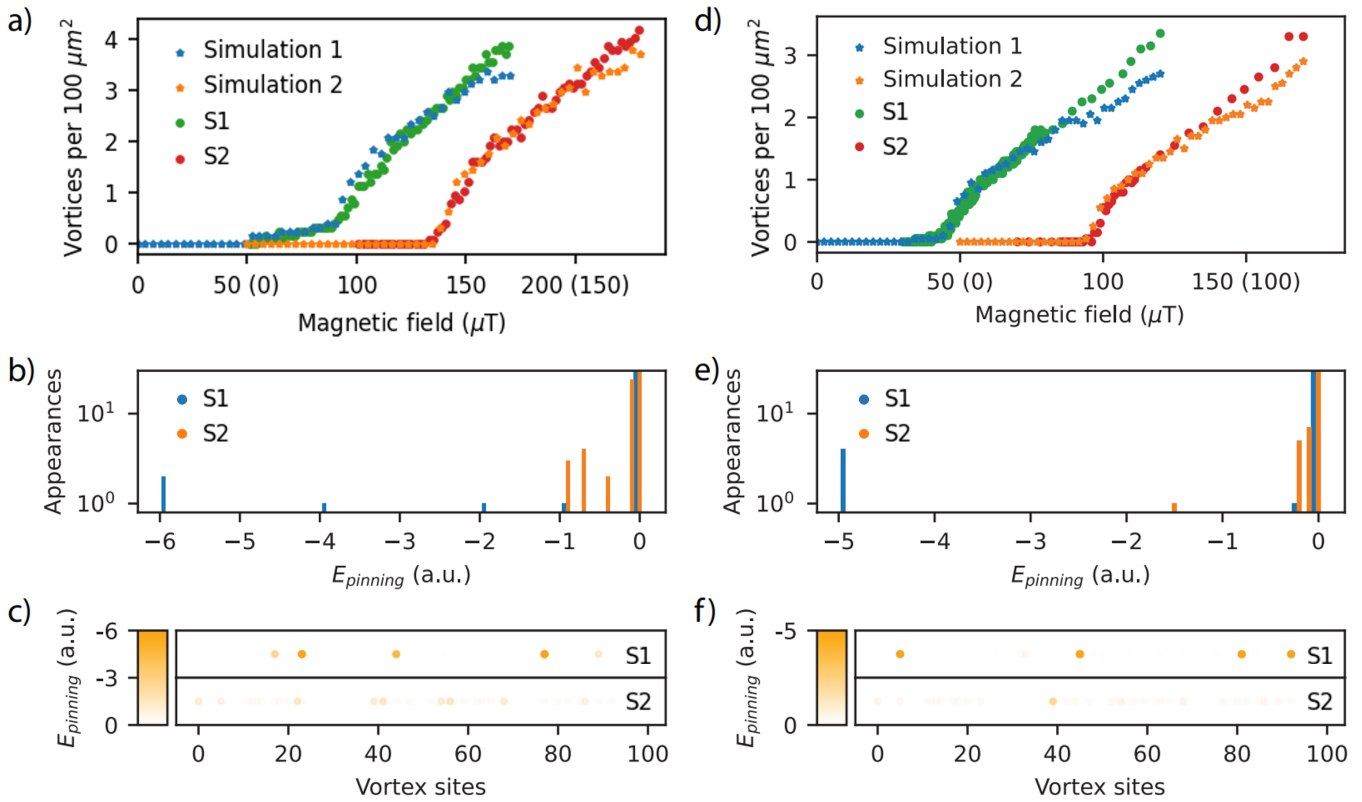


**FIG. 6:** a) Comparison between Monte Carlo simulations and experimental data for the  $7\mu\text{m}$  strips from S1 and S2. Results for S2 are shifted by  $50\mu\text{T}$ , as indicated by axis labels in brackets. b) Histogram of pinning energy distribution for the 100 allowed sites along the strip. c) Pinning energy configurations for S1 (top) and S2 (bottom); darker dots indicate stronger pinning sites. (d-f) Analogous results for the  $10\mu\text{m}$  strips from S1 and S2.

$r_c = 190\text{ nm}$  is assumed for  $10\mu\text{m}$  strips. We obtain good agreement with the experimental data up to the field at which a second row of vortices begins to form - around  $150\mu\text{T}$  for the  $7\mu\text{m}$  strip and approximately  $90\mu\text{T}$  for the  $10\mu\text{m}$  strip. The pinning site density and energy distribution are shown in Fig. 6 b) and e) on a common axis for both samples. Figs. 6 c) and f) show the randomly generated realizations of the pinning configuration used in the simulations. Notably, to capture the shallow tails in the curves, S1 requires pinning sites with higher energies but low density. To account for the broadening of the shoulder pinning sites with lower energy but higher density are needed. These differences between S1 and S2 reflect variations in the pinning landscape across the wafer that both samples originate from.

A limitation of our simulations is that they are based on a one-dimensional toy model. However, the images indicate that even before a second row forms in the strips, some vortices appear off-center. In principle, a full two-dimensional simulation using a time-dependent Ginzburg-Landau approach - with an appropriately tuned pinning landscape - could capture these details more accurately and also account for the dynamics of vortices while the sample is cooled. However, this level of modeling is beyond the scope of this work.

## VI. CONCLUSION

We imaged NbTiN superconducting strips cooled in magnetic field to study their vortex trapping properties. In addition to analyzing the threshold field at which the first vortex enters, we present detailed experimental data and modeling that explore the behavior of vortices above threshold field. Our measurements clearly resolve expected features - specifically, an initially step increase in vortex number that softens once the vortex spacing approaches the strip width. We also clearly observe signature of pinning effects, which we explore in two different samples and capture using a one-dimensional model solved via Monte Carlo simulations.

Our models, based on the Gibbs free energy of point-like vortices and localized pinning sites, capture many aspects of the vortex behavior in these strips. However, discrepancies remain, such as the variation of the optimal vortex core radius,  $r_c$ , with the applied magnetic field. We also note that the threshold field for our  $10\mu\text{m}$  strips is lower than that observed in a Nb film[1], despite Nb's longer low-temperature coherence length relative to NbTiN. Overall, these observations suggests that kinetic effects during field cooling - which are not accounted for in current models including ours - play a significant role,

and that a more detailed investigation of pinning effects is needed.

Future work will extend our models to incorporate kinetic effects and a more detailed treatment of pinning. Experiments that explicitly characterize vortex freezing, pinning strength, and the impact of cooling protocols will be essential to guide these efforts. In addition, side-by-side comparisons of strips made from different superconducting films (e.g., Nb and NbTiN) under identical experimental conditions will help clarify the relationship between the effective  $r_c$  used in our models and the low-temperature coherence length.

## ACKNOWLEDGMENTS

Research was partially sponsored by the U.S. Department of Energy, Office of Science, Offices of Nuclear Physics and Advanced Scientific Computing Research under contract DE-AC05-06OR23177, and by the Army Research Office under Grant Number W911NF-24-1-0150. Initial scanning SQUID measurements were also supported by the Cornell Center for Materials Research with funding from the NSF MRSEC program (DMR-1719875). Sample design and fabrication at imec and imec USA were also supported by imec INVEST+ and by Osceola County. AMVF acknowledges support by the U.S. Department of Energy, Office of Science, and Office of Nuclear Physics under Contract No. DE-AC05-06OR23177.

- 
- [1] Gheorghe Stan, Stuart B. Field, and John M. Martinis. Critical field for complete vortex expulsion from narrow superconducting strips. *Physical Review Letters*, 92(9):097003, Mar 2004.
- [2] K. H. Kuit, J. R. Kirtley, W. van der Veur, C. G. Moleenaar, F. J. G. Roesthuis, A. G. P. Troeman, J. R. Clem, H. Hilgenkamp, H. Rogalla, and J. Flokstra. Vortex trapping and expulsion in thin-film  $\text{YBa}_2\text{Cu}_3\text{O}_{7-\delta}$  strips. *Phys. Rev. B*, 77:134504, Apr 2008.
- [3] L. Ceccarelli, D. Vasyukov, M. Wyss, G. Romagnoli, N. Rossi, L. Moser, and M. Poggio. Imaging pinning and expulsion of individual superconducting vortices in amorphous MoSi thin films. 100(10):104504.
- [4] Jun-Yi Ge, Vladimir N Gladilin, Joris Van de Vondel, and Victor V Moshchalkov. Vortex matter and critical magnetic fields in mesoscopic superconducting strips. *Superconductor Science and Technology*, 36(8):085014, jul 2023.
- [5] Eric Bronson, Martin P. Gelfand, and Stuart B. Field. Equilibrium configurations of pearl vortices in narrow strips. *Phys. Rev. B*, 73:144501, Apr 2006.
- [6] See Supplemental Material at URL-will-be-inserted-by-publisher .
- [7] Ankit Pokhrel, Daniel Pérez Lozano, Jean-Philippe Soulié, Diziana Vangoidsenhoven, Sujan K. Sarkar, Rajendra K. Saroj, Yann Canvel, Vincent Renaud, Bart Kenens, Amey M. Walke, Jasper Bizindavyi, Sara Iraci, Seifallah Ibrahim, Blake Hodges, Trent Josephsen, Manu Perumkunnil, Benjamin Huet, Sabine O’Neal, Quentin Herr, Zsolt Tókei, and Anna Herr. Nbtin based two-metal level semi-damascene interconnects, josephson junctions and capacitors for superconducting digital logic. In *2024 IEEE International Electron Devices Meeting (IEDM)*, pages 1–4, 2024.
- [8] Sara Iraci, Ankit Pokhrel, Daniel Perez Lozano, Jean-Philippe Soulié, Sujan Kumar Sarkar, Rajendra Kumar Saroj, Yann Canvel, Vincent Renaud, Amey Mahadev Walke, Bart Kenens, Blake Hodges, Seifallah Ibrahim, Trent Josephsen, Benjamin Huet, Gayle Murdoch, Min-Soo Kim, Sabine O’Neal, Quentin Herr, Anna Herr, and Zsolt Tókei. Two metal level semi-damascene interconnects for superconducting digital logic. In *2024 IEEE International Interconnect Technology Conference (IITC)*, pages 1–3, 2024.
- [9] Daniel Pérez Lozano, Jean-Philippe Soulié, Blake Hodges, Xiaoyu Piao, Sabine O’Neal, Anne-Marie Valente-Feliciano, Quentin Herr, Zsolt Tókei, Min-Soo Kim, and Anna Herr. Properties of nbxti(1-x)n thin films deposited on 300 mm silicon wafers for upscaling superconducting digital circuits. *Superconductor Science and Technology*, 37(7):075012, June 2024.
- [10] Anna Herr and et. al. Scaling superconducting fabrication processes to 400m devices/cm2 and compute density comparable to advanced-node cmos. *Frontiers in Materials*, In review.
- [11] Holger Bartolf. *Fluctuation Mechanisms in Superconductors*, pages 181–184. Springer Fachmedien Wiesbaden, Wiesbaden, 2016.
- [12] Martin E. Huber, Nicholas C. Koshnick, Hendrik Bluhm, Leonard J. Archuleta, Tommy Azua, Per G. Björnsson, Brian W. Gardner, Sean T. Halloran, Erik A. Lucero, and Kathryn A. Moler. Gradiometric micro-squid susceptometer for scanning measurements of mesoscopic samples. *Review of Scientific Instruments*, 79(5):053704, May 2008.
- [13] John R. Kirtley, Lisa Paulius, Aaron J. Rosenberg, Johanna C. Palmstrom, Connor M. Holland, Eric M. Spanton, Daniel Schiessl, Colin L. Jermain, Jonathan Gibbons, Y.-K.-K. Fung, Martin E. Huber, Daniel C. Ralph, Mark B. Ketchen, Jr. Gibson, Gerald W., and Kathryn A. Moler. Scanning squid susceptometers with sub-micron spatial resolution. *Review of Scientific Instruments*, 87(9):093702, Sep 2016.
- [14] J. Pearl. Current distribution in superconducting films carrying quantized fluxoids. *Appl. Phys. Lett.*, 5(4):65–66, 11 1964.
- [15] Vladimir G. Kogan. Pearl’s vortex near the film edge. *Phys. Rev. B*, 49:15874–15878, Jun 1994.
- [16] John Bardeen. Quantization of flux in a superconducting cylinder. *Phys. Rev. Lett.*, 7:162–163, 1961.
- [17] K. K. Likharev. The formation of a mixed state in planar semiconductor films. *Radiophysics and Quantum Electronics*, 14(6):722–727, June 1971.
- [18] J. R. Clem. *Bull. Am. Phys. Soc.*, 43(401), 1998.